Lattice-mismatched heteroepitaxy of IV-VI thin films on PbTe(001): An *ab initio* study

Chang-Eun Kim,[1] Young-Joo Tak,[1] Keith T. Butler,[2] Aron Walsh,[2,1] and Aloysius Soon[1,2,*]

[1]*Global E³ Institute and Department of Materials Science and Engineering, Yonsei University, Seoul, Korea*

[2]*Centre for Sustainable Chemical Technologies and Department of Chemistry, University of Bath, Bath, United Kingdom*

(Received 4 December 2014; revised manuscript received 25 January 2015; published 17 February 2015)

The chalcogenides of tin and lead (SnS, SnSe, SnTe, PbS, PbSe, and PbTe) have applications ranging from solar cells to thermoelectrics. Taking rocksalt structured PbTe(001) as the substrate, we explore the coherent (001)-oriented heteroepitaxy of the other five IV-VI semiconductors through first-principles electronic structure calculations. We investigate the effects of lattice strain and its relationship to the interface energy, as well as the electron redistribution, as a function of the epilayer thickness [from 1 to 5 monolayers (ML)] below the dislocation critical point. Analysis of the chemical bonding explains trends including work function shifts and surface rumpling. Among the five combinations studied SnTe/PbTe(001) has the smallest lattice mismatch, resulting in the most stable coherent interface and unique charge transfer behavior. Here, we perform orbital-resolved band structure calculations (with spin-orbit coupling effects) for the SnTe/PbTe(001) system, highlighting its potential use in topological spintronic thin-film devices.

DOI: 10.1103/PhysRevB.91.085307 PACS number(s): 68.35.Ct, 68.35.Md, 68.37.Lp, 68.65.Hb

I. INTRODUCTION

IV-VI semiconductor compounds are used in a variety of technological applications including infrared (IR) radiation sensors, quantum dot grids, and thermoelectric devices [1–3]. In these applications the control of surfaces and interfaces is of critical importance for the incorporation of target materials into working devices. Monolayer fabrication techniques have matured to the extent that synthesis of materials layer by layer is achievable. The accessibility of such extreme dimensionality has resulted in the observation of many unique properties.

Surfaces and interfaces of IV-VI nanocomposites have attracted much attention due to their unique properties. For example, the PbSe/$Pb_{1-x}Eu_xTe$ system is known to form well defined quantum dots, mainly caused by the intrinsic stability of {100} facets of their lattice structures [4]. The fundamental understanding of the interfaces and surfaces plays a crucial role to explore the unique property of nanocomposites. A firm understanding of the atomistic and electronic structure of a material is crucial to the exploitation of the unique properties of ultrathin films and related nanostructures.

Density functional theory (DFT) has been successfully applied to understanding the solid-state systems in a number of contexts. In this study we consider the interface between ultrathin films of a series of tin and lead chalcogenides on a PbTe substrate. Investigating the structural and energetic properties of these systems presents a number of computational challenges related to the nature of their coherent but strained interfaces.

Similar to other rocksalt structures [5], PbTe has been shown experimentally to exhibit a surface rumpling behavior, with Te atoms relaxing out of the surface and Pb atoms relaxing inwards [6]. Previous computational work on the (001) surface of PbTe has also demonstrated rumpling patterns [7].

The heteroepitaxy film systems of IV-VI/PbTe(001) are interesting because they play a role as an ideal model for understanding the interfaces of the initial stage of growing quantum dot nanostructures. As exemplified in the PbTe/PbSe(001) quantum dot system [8], the residual strain in their interface regime causes a dislocation pattern along [110] and [$\bar{1}$10] directions, inducing formation of quantum dots. Complementing this, a recent experimental study [9] on the effect of compressive strain on SnTe-supported PbTe thin films also demonstrated that dislocation patterns will begin to appear when the thin film thickness exceeds 20 Å, which roughly corresponds to six to seven monolayers of PbTe. For those quantum dots systems, fine control of the size and distribution of the unit cell is one of the key elements to achieve next generation quantum devices. Therefore, understanding the fundamental properties of the strain and coherency of the interface between growing thin film and the substrate is of both fundamental and technological importance. Also, while the compressive strain effects on the quantum dot formation on the PbTe(001) have been extensively investigated, the role of extensive strain to these interfaces is still not well understood.

Strained but coherent interfaces are also known to play a crucial role to enhancing the figure of merit in thermoelectric devices [10,11]. When it comes to endotaxial interface structures, enhanced phonon scattering was observed while the electrical conductivity of the system was preserved due to coherency of the interface.

In this study, we will present a set of systematic calculations toward the understanding of the strained coherent interfaces of IV-VI/PbTe(001) systems (where IV=Pb, and Sn, and VI=S, Se, and Te). The heteroepitaxy systems modeled and studied in this work present various lattice mismatch ratios with different interface chemistries, thereby providing an interesting approach to understanding these strained interfaces between IV-VI composites and the PbTe(001) substrate. (See Fig. 1.) Moreover, the fundamental understanding gained in this work will also afford much insight on the role of geometric strain and interface chemistries upon the endotaxial growth mode on PbTe(001) for potential high-efficiency thermoelectrics. This study also provides insight towards understanding endotaxial

*aloysius.soon@yonsei.ac.kr

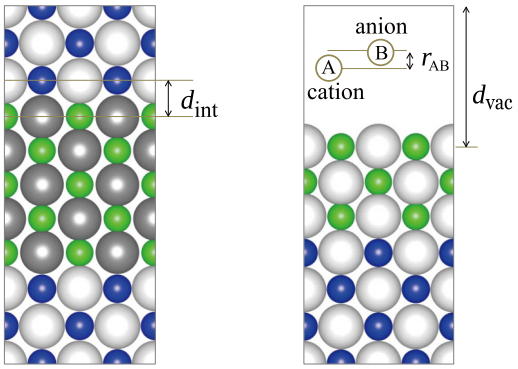

(a) Interface model (SnSe| PbTe) (b) Thin film model (3ML PbSe/PbTe)

FIG. 1. (Color online) (a) Example of the interface model used in the study. Sandwich type slab model with five monolayer (ML) thickness for each element has been used. (b) An example of the film-substrate model in the study. IV-VI semiconductor compounds thin films were constructed coherently on PbTe(001), resulting in lateral strain of the thin film. A vacuum region (d_{vac}) of 18 Å is employed for the slab models.

interfaces of chalcogenide systems where formation of coherent but strained interfaces are expected [11].

II. METHODOLOGY

DFT calculations are performed within generalized gradient approximation (GGA), with the PBE (Perdew-Burke-Ernzerhof) exchange-correlation (xc) functional [12,13], as implemented in the Vienna *ab initio* simulation package (VASP) [14,15]. The kinetic energy cutoff for the plane wave basis set is set to 500 eV and the electron-ion interactions are represented by the projector augmented wave (PAW) potentials [16,17].

In passing, we find that applying van der Waals correction (namely, the D2 Grimme's scheme for London dispersion as implemented in VASP) to our DFT total energies is required to obtain the correct phase order of SnS. It is known that the stable ground-state structure for both SnS and SnSe is a distorted rocksalt structure with the $Pbnm$ symmetry, and transforms to $Cmcm$ at elevated pressures and temperatures [18]. The phase deformation/transformation for both SnS and SnSe is outside of the scope in this work. Here, we focus on how such large lattice mismatch contributes to destabilizing the interface without explicit corrections for the weak van der Waals interactions.

Monkhorst-Pack [19] type **k** points are used for all calculations, which were carefully tested for convergence (i.e., total energies are converged within 5 meV per atom using an $8 \times 8 \times 8$ **k** grid for bulk systems, and an $8 \times 8 \times 1$ **k** grid for surface or interface models). For all surface and interface models, a vacuum region of 18 Å is employed. The interface supercell symmetric slab model is constructed using 11 atomic layers of PbTe in the (001) direction. The thickness of adlayer thin films are then varied from 1 to 5 ML on each side of the slab. The coordinates of PbTe atoms in the three innermost atomic layers are fixed to their bulk positions, and all other atoms are then allowed to be fully relaxed. To account for the surface rumpling behavior in these B1 thin films, we have also measured the relative displacement of the cation-anion positions, r^j_{AB}, by calculating $r^j_{\text{AB}} = z^j_{\text{A}} - z^j_{\text{B}}$, where z^j is the z-coordinate displacement of either the A or B atom on the outermost surface.

In this work, we define the bulk strain energy, $E^{\text{str}}_{\text{AB}}$, as

$$E^{\text{str}}_{\text{AB}} = E^{\text{str-bulk}}_{\text{AB}} - E^{\text{bulk}}_{\text{AB}}, \tag{1}$$

where $E^{\text{str-bulk}}_{\text{AB}}$ is the total energy of strained AB bulk structure at its laterally strained geometry, while $E^{\text{bulk}}_{\text{AB}}$ is the total energy of AB bulk structure in its original optimized geometry. Throughout this work, "AB" will be used as a synonym for "IV-VI" compounds for brevity, and the terms will be used interchangeably.

Next, we determine the adsorption energy of AB on PbTe(001), E_{ad}, via

$$E_{\text{ad}} = \frac{\left(E_{\text{AB/PbTe}} - E_{\text{PbTe(001)}} - 2n_{\text{AB}}E^{\text{mlc}}_{\text{AB}}\right)}{2n_{\text{AB}}}, \tag{2}$$

where $E_{\text{AB/PbTe}}$ is the total energy of the AB/PbTe(001) interface structure, $E_{\text{PbTe(001)}}$ the total energy of the PbTe(001) substrate, n_{AB} the thickness of AB adlayers (n.b. the factor 2 accounts for the formation of the AB thin film on both sides of the symmetric supercell slab model), and $E^{\text{mlc}}_{\text{AB}}$ the total energy of the reference AB diatomic molecule in the gas phase. The choice of this reference state is common in growth experiments of these IV-VI thin films.

To investigate the formation and thermodynamic stability of these heteroepitaxial AB thin films on PbTe(001), we propose two ways of calculating the formation energy of these AB/PbTe(001) thin films, E^{f} [20]. First, we define $E^{\text{f}}(n_{\text{AB}})$ as

$$E^{\text{f}}(n_{\text{AB}}) = \frac{\left(E_{\text{AB/PbTe}} - E_{\text{PbTe(001)}} - 2n_{\text{AB}}E^{\text{str-bulk}}_{\text{AB}}\right)}{2}, \tag{3}$$

where the term $E^{\text{str-bulk}}_{\text{AB}}$ may be obtained from Eq. (1).

The second (albeit, more *indirect*) way to calculate $E^{\text{f}}(h)$ as a function of film thickness h can be expressed as

$$E^{\text{f}}(h) = \sigma^{\text{str}}_{\text{AB}} - \sigma_{\text{PbTe}} + E^{\text{int}} + hE^{\text{str}}_{\text{AB}}, \tag{4}$$

where both $\sigma^{\text{str}}_{\text{AB}}$ and σ_{PbTe} are the surface energies of the strained AB film and that of the PbTe(001) substrate, respectively. Here, E^{int} is the interface energy given by

$$E^{\text{int}} = \frac{E_{\text{AB/PbTe}} - n_{\text{AB}}\left(E^{\text{str}}_{\text{AB}} + E^{\text{bulk}}_{\text{AB}}\right) - n_{\text{PbTe}}E^{\text{bulk}}_{\text{PbTe}}}{2A}, \tag{5}$$

where n_{PbTe} and $E^{\text{bulk}}_{\text{PbTe}}$ are the number of PbTe formula units in the PbTe(001) substrate and the total energy of bulk PbTe, respectively. And here A is taken as the surface area of the interface system.

With regards to the electronic structure of these systems, we study the dependence of the work function change on the adlayer thickness, calculated with respect to the surface work function of pristine PbTe(001). To better understand the nature of interfacial bonding mechanism as a function of film thickness, we also consider the difference electron density plots of these interfaces with increasing film thickness. Using the most stable SnTe/PbTe(001) system, we have also calculated orbital-resolved electronic interface band structures for 3 ML SnTe/PbTe(001) to illustrate the interplay between

TABLE I. DFT-optimized lattice constant, a_0, of the respective B1-structured IV-VI compounds used in this work (provided in Å). Other experimental [21,22] and theoretical values [22–25] found in literature are also listed for comparison. The percentage errors (compared to available experimental values) are provided in the parentheses.

a_0 (in Å)	This work	LDA[a]	GGA-PW91[b]	Experiment[c]
SnS (B1)	5.848	5.698	5.848	
SnSe (B1)	6.061	5.904	6.062	
SnTe	6.407 (1.5%)	6.242	6.312	6.313
PbS	6.008 (1.3%)	5.906	5.992	5.929
PbSe	6.217 (1.6%)	6.098	6.20	6.117
PbTe	6.567 (1.9%)	6.439	6.556	6.443

[a]References [22,24].
[b]References [23,25].
[c]References [21,22].

strong oscillatory features in its electronic structure. Here, we have included the relativistic noncollinear spin-orbit coupling terms.

III. RESULTS AND DISCUSSION

A. Bulk and surface atomic structure

In Table I, we report the lattice constants of bulk SnS, SnSe, SnTe, PbS, PbSe, and PbTe crystallized in the cubic B1 rocksalt structure. We note that both SnS and SnSe crystallize naturally in the orthorhombic *Pbnm* symmetry rather than the B1 structure [18]. The lower symmetry structure is associated with the stereochemical activity of the Sn $5s^2$ lone pair. For this work, both materials are grown coherently on PbTe(001) in the metastable B1 structure, allowing only atomic relaxations in the z axis. Our calculated lattice constants are well within 2% error of the experimental references. The thermal lattice dynamics in B1-type bulk materials (namely, PbS, PbSe, and PbTe) has been recently reported [26] and will not be explicitly considered here. It is found that these materials have very similar thermal expansion coefficients at around 300 to 400 °C and this temperature range is typical, for example, for the growth of lattice-mismatched quantum dots [27,28]. In addition, the bulk moduli of these B1 compounds are softened by about 10% at elevated temperatures which may contribute to attenuating the interfacial stress experienced in these ultrathin nanofilms.

To study the effect of lateral extensive strain to these ultrathin adlayer films, we then strain the a-b plane of these adlayer IV-VI materials to match that of PbTe. When this strain is applied, the relaxed c parameters are found from the minimization of the total energy-constrained volume calculations, i.e., $\partial E_{\rm tot}/\partial c_{\rm str} = 0$, where $E_{\rm tot}$ is the total energy of the strained bulk model, and $c_{\rm str}$ is the strained c axis parameter, while a and b are fixed to those of PbTe substrate. In Fig. 2(a), this is illustrated and we compare our results with the commonly used volume conservation approximation approach (shown as the vertical dotted line). It can be seen that such simplistic approximation resulted in both an underestimated volume which could then lead to an overestimation of the strain energy.

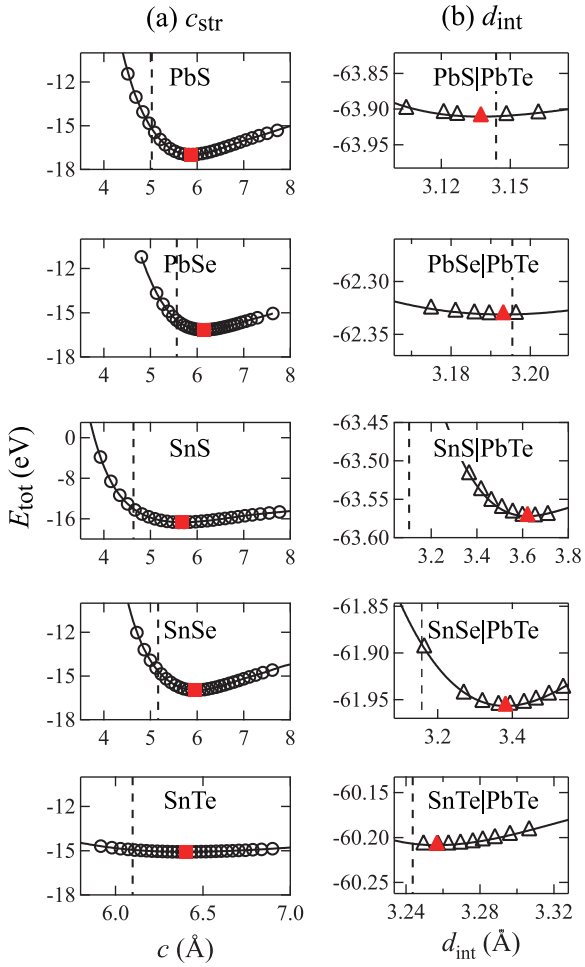

FIG. 2. (Color online) (a) Total energy of strained bulk structure as its a and b lattice parameters are fixed to those of PbTe(001) and c is allowed to vary as given on the abscissa. (b) Total energy from geometric optimization for the strained interface models. The minimum values were found from polynomial fit to the energy-distance data.

To further illustrate the failure of yet another commonly used arithmetic averaging of the interlayer distance approach, we show in Fig. 2(b) that this simple averaging method could lead to an inaccurate description of interlayer distances (though the error in total energy was not large). Using our approach, we find the optimized c parameters for the adlayer materials SnS, SnSe, SnTe, PbS, and PbSe to be 5.675, 5.965, 6.402, 5.865, and 6.143 Å, respectively.

Experimentally, He *et al.* [29] studied the geometry of PbS clusters in a PbTe matrix, and found that the PbS/PbTe system forms coherent interfaces along {001} planes. From a cross-section HR-TEM image, they measured and found the interlayer distance to be in the range of 6.02 to 6.40 Å, closely agreeing with our calculated value of 6.28 Å.

The calculated interlayer rumpling, $r^{\rm AB}$, as a function of adlayer thickness is shown in Fig. 3. In addition, we correlate the observed trends with increasing lattice misfit ratio, m. We define this misfit ratio, m, of compound AB as $m = (a^{\rm PbTe} - a^{\rm AB})/a^{\rm AB}$. To aid our discussion, we show the averaged rumpling observed for the strained AB layers (strain

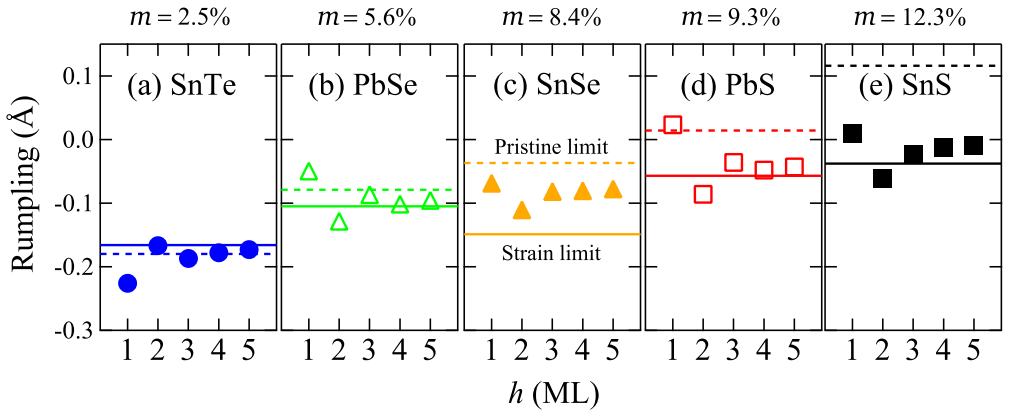

FIG. 3. (Color online) Rumpling behavior of the outermost layer of the adlayer systems with respect to varying thickness. Solid line denotes the rumpling effect observed for the strained AB layers (strain limit), while the broken line denotes the rumpling of the strain-free AB layers. The misfit ratio m of compound AB is defined as $m = (a^{\mathrm{PbTe}} - a^{\mathrm{AB}})/a^{\mathrm{AB}}$.

limit) in solid horizontal lines, while that of the strain-free AB layers in dashed horizontal lines. Generally, we find a convergence of the rumpling behavior of these ultrathin adlayer nanofilms towards that of the strained pristine IV-VI slab models is observed with increasing adlayer thickness. At the ultrathin limit (1 to 2 ML), they exhibit larger fluctuations and plateau for nanofilms thicker than 3 ML to their strain limit. It is also clearly seen in Fig. 3 that the difference between the two horizontal lines (i.e., the averaged rumpling observed for the strained and strain-free AB adlayers) widens as the misfit ratio, m, increases. This is particularly severe for SnS and SnSe, we rationalize this as being a consequence of its natural orthorhombic crystal structure (rather than the B1 used in this discussion).

Surface rumpling is commonly observed for many B1-structured materials, particularly in the (001) direction [5]. Considering only the pristine PbTe(001) surface, we calculate this interlayer rumpling to be $r^{12} = -0.2$ Å with the Te anion displacing out of the surface. This is in fair agreement with reported low energy electron diffraction (LEED) experiments [6,30] and other DFT calculations [7].

B. Interface thermodynamics

To assess the interface thermodynamics of these ultrathin IV-VI nanofilms on PbTe(001), we first calculate their adlayer strain energy [$E^{\mathrm{str}}_{\mathrm{AB}}$; cf. Eq. (1)] and adsorption energy [E_{ad}; cf. Eq. (2)] to understand how strongly they "bind" on the PbTe(001) substrate. We find both energies depend largely on the difference between adlayer and substrate lattice constants: the misfit ratio, m. To illustrate this, the strain energy and adlayer adsorption energy for 1 ML IV-VI/PbTe(001) structures are plotted in Figs. 4(a) and 4(b), respectively. It is clear from Fig. 4 that $E^{\mathrm{str}}_{\mathrm{AB}}$ increases as the misfit ratio, m, increases. On the other hand, E_{ad} of the various IV-VI adlayers seem to generally decrease (i.e., become more positive) with increasing m.

To study the formation energy of these ultrathin nanofilm adlayers on PbTe(001), we have adopted the calculation of this energy term using both a "direct" approach [cf. Eq. (3)] as well as an "indirect" phenomenological approach [cf. Eq. (4)] as outlined in Ref. [20]. The main difference lies in the $E^{\mathrm{i-s}}$ term, which describes the interaction between the exposed surface and interface region. This term is found to strongly affect the thin film energetics at extremely low dimensions (e.g., a few atomic layers thick) [20]. The calculated IV-VI/PbTe(001) formation energy based on these two approaches is plotted in Fig. 5. Here, the direct method [cf. Eq. (3)] is shown as markers, while the indirect empirical relation [cf. Eq. (4)] is plotted as solid straight lines. In addition to the $E^{\mathrm{str}}_{\mathrm{AB}}$ energy term, one would also require the surface energy of the strained adlayer surfaces, $\sigma^{\mathrm{str}}_{\mathrm{AB}}$ which are listed in Table II. In comparison to the III-V materials studied in Ref. [20], we find that the B1 IV-VI compounds in this study do not show a large $E^{\mathrm{i-s}}$ term for the ultrathin adlayers.

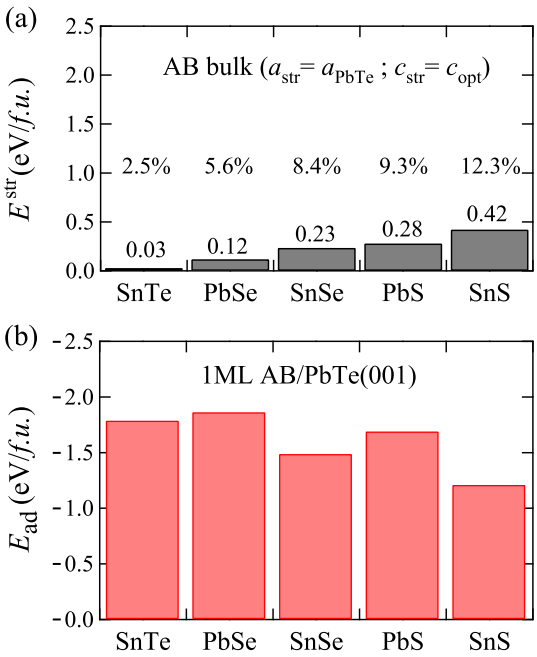

FIG. 4. (Color online) (a) Strain energy, $E^{\mathrm{str}}_{\mathrm{AB}}$ [cf. Eq. (1)] where the inset numbers represent the misfit ratio, m, and (b) E_{ad} [cf. Eq. (2)] for 1 ML IV-VI/PbTe(001). The negative signs in the vertical axis indicate that the reaction is exothermic with respect to the isolated binary IV-VI molecules.

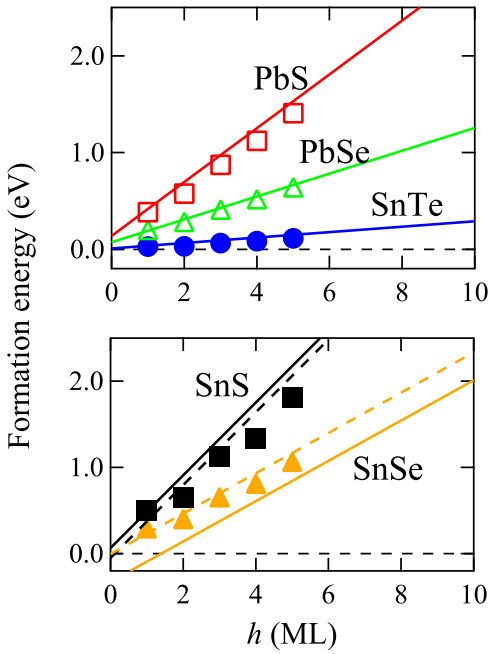

FIG. 5. (Color online) Adlayer formation energy, calculated from direct total energy calculation (markers) and indirect thermodynamic model calculation (solid line). The additional lines for SnS and SnSe correspond to an indirect calculation with the unrelaxed surface energy.

We note that SnS and SnSe do not agree as well (see lower panel in Fig. 5) between the two approaches unless the energy from unrelaxed structures are used instead. This suggests that orthorhombic structured SnS and SnSe experience an additional energetic deviation that comes from a structural incompatibility with rocksalt when the atomic geometry was allowed to relax. As the adlayer grows thicker, the energetic penalty due to accumulated stress increases linearly until it triggers structural deformation. This highlights an important technical consideration when using the indirect form of film formation energy model to investigate strained interface, which may not be capable of capturing the structural effect accurately. In Fig. 5, the dashed lines for the SnS and SnSe cases are obtained by suppressing the structural relaxation in their rocksalt pristine structures, which then produce a better agreement with the direct method since SnS and SnSe have a strong tendency to surface reconstruction, as discussed earlier in the section.

An experimental study [9] was conducted to study the effect of compressive strain to a PbTe thin film on a SnTe substrate. They report that dislocation pattern began to appear as the thickness exceeded 20 Å, which roughly corresponds to six or seven monolayers of SnTe. The authors considered a compressively strained system; still we can compare this to our expansively strained case of SnTe/PbTe(001). In the elastic regime, we can assume the energy gain due to compressive strain is comparable to the strain energy due to expansive strain, which allows us to find that the thickness of SnTe film used in this work falls below the critical thickness of the observed dislocation. On the other hand, this also suggests that most of the other thin film models used in the study may be prone to surface reconstruction in experimental systems. When it comes to a sub-nano-dimension materials system where experimental characterization is hard and expensive, such theoretical estimation as presented in this work may provide a valuable insight to selectively perform effective experimental and theoretical studies.

TABLE II. Surface energy of strained pristine B1 structures. Surface energy σ is calculated from strain-free rocksalt pristine structures, while σ^{str} is derived from the strained pristine structures.

	SnTe	PbS	PbSe	PbTe
σ (meV/Å^2)	10.0	11.2	11.0	10.2
σ^{str} (meV/Å^2)	9.3	12.0	10.9	

The most stable SnTe/PbTe(001) thin film structure is chosen for an in-depth theoretical investigation regarding various interesting physical properties. A careful theoretical study on SnTe thin films suggested that a nontrivial two-dimensional topological crystalline insulator (2D TCI) phase arises as the thickness increases [31]. This work suggests that the 2D TCI phase appears as the thickness approaches 5 ML, and this topological character becomes more pronounced as the thickness reaches 25 ML. While this gives an optimistic insight for a realization of 2D TCI devices, our calculation results caution that one should/must carefully choose a suitable substrate with minimal lattice misfit ratio m, and surface relaxation effects should not be neglected. Such geometric concerns are found to be quite important factors which affect the delicate electronic properties of topological materials. We also discussed an effect coming from variations in the stacking order to the topological state of the thin film recently [32]. Based on the results in this work, we suggest PbTe(001) as a suitable growth substrate for SnTe, due to the minimal lattice mismatch among various combinations in IV-VI materials. In fact, we corroborate well with recent results by Yang *et al.* [33], where they studied the SnTe(001)/PbTe(001) interface and found nontrivial Chern numbers in weak definitions. This will be discussed later in the section with related calculation results.

C. Electronic structure

Turning now to the electronic structure of these IV-VI/PbTe(001) nanofilms, we report the thickness-dependent surface work function change, $\Delta\Phi$ [i.e., calculated with respect to that of pristine PbTe(001)] in Fig. 6. Here the work function is determined as the energy difference between the vacuum level and the top of the valence band, and is equivalent to the surface ionization potential. We find two distinct cation-dependent trends as a function of adlayer thickness—Pb-based chalcogenide adlayers exhibit strong layer-dependent alternating $\Delta\Phi$ values (see left panel of Fig. 6), while Sn-based chalcogenide adlayers show a less pronounced trend (i.e., gently decreasing with thickness; see left panel of Fig. 6). It is evident that the chemical character of the cation plays an important role in its electronic structure. This alternating trend in $\Delta\Phi$ (as well as in r^j_{AB}, reported above) warrants a deeper study. In a recent theoretical study,

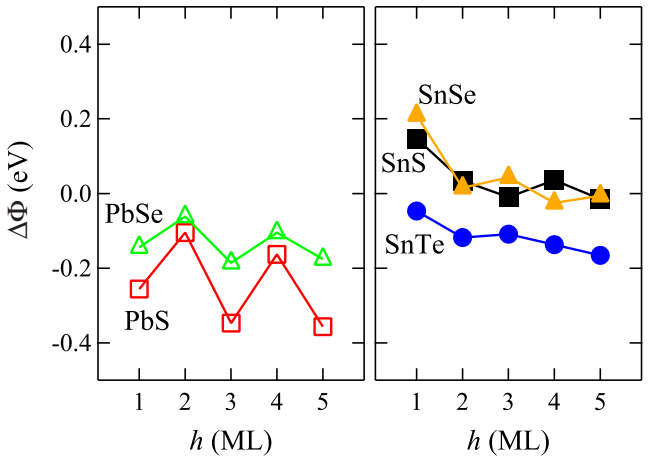

FIG. 6. (Color online) Calculated work function change of PbTe(001) due to thin film formation.

the thickness dependent behavior in the electrostatic potential was considered as a part of design rules for a novel transparent conducting oxide [34].

Thus, to further investigate the nature of the bonding mechanism at the interface as a function of adlayer thickness, we plot the difference electron density plots for these IV-VI/PbTe(001) systems in Fig. 7. These plots are defined as the difference between the total charge densities of the adlayer/substrate system, the substrate PbTe(001), and that of the individual atoms in the adlayer. As seen in Fig. 7, the response of the adlayer to the substrate-induced strain is not solely determined by the magnitude of the strain energy, but is also drastically affected by the chemical nature of the anion in the adlayer. Anions with strong stereochemical activity (e.g., S and Se) clearly show thickness-dependent *interlayer dimerization* as a response to the expansive strain. This thickness-dependent dimerizing behavior sensitively influences the adlayer-substrate charge transfer—strongly for odd-layered nanofilms and weakly for even-layered nanofilms. This expansive substrate-induced stress mechanism then explains the alternating trends seen in both $\Delta\Phi$, as well as r^j_{AB}. For instance, in the case of SnTe/PbTe(001), where one sees the weakest dimerization effect due to the lowest misfit ratio of 2.5%, the variation of both $\Delta\Phi$ and r^j_{AB} are less pronounced.

From previous studies, it was shown that bulk SnTe is a TCI and its topological features of the electronic structure are kept by inversion symmetry [35]. In rocksalt crystal structures, the inversion symmetry exists along the diagonal axes. In the SnTe/PbTe(001) nanofilm interface system, the same symmetry does not exist and is broken by the creation of this interface. However, a recent study found that their nontrivial electronic structure along (001) orientation is defined by weak definition of the mirror Chern numbers [31]. To further explore the SnTe/PbTe(001) nanofilm system, we calculate and plot the orbital-resolved electronic interface band structure of 3 ML SnTe/PbTe(001) in Fig. 8, weighted by each orbital projection to the total wave function. Here we find a massless Dirac-cone shape crossing the Fermi level, indicating the Sn $5s$ and $5p$ orbitals strongly contribute to the metallic state of this

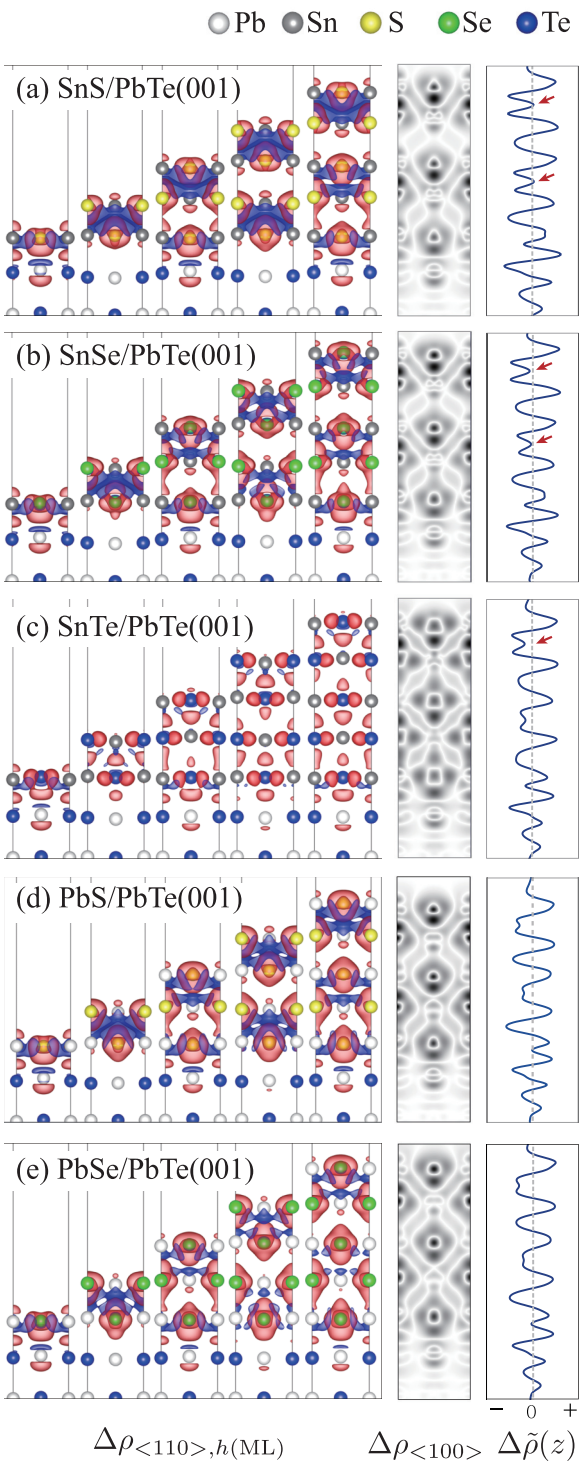

FIG. 7. (Color online) Charge difference plot showing the electronic density redistribution due to the chemical interaction between the components. The red color indicates accumulation; blue color shows depletion in the electronic density. The 2D cross section images of (100) plane and planar-averaged data along the z axis [$\Delta\tilde{\rho}(z)$] are shown for comparison. The red arrows point to the characteristic peaks indicating strong dimerizations.

SnTe/PbTe(001) nanofilm system, suggesting the character of a $s-p$ type topological insulator.

Considering the pristine SnTe system, as seen in Figs. 8(a) and 8(b), expansive substrate-free strain opens up the band gap

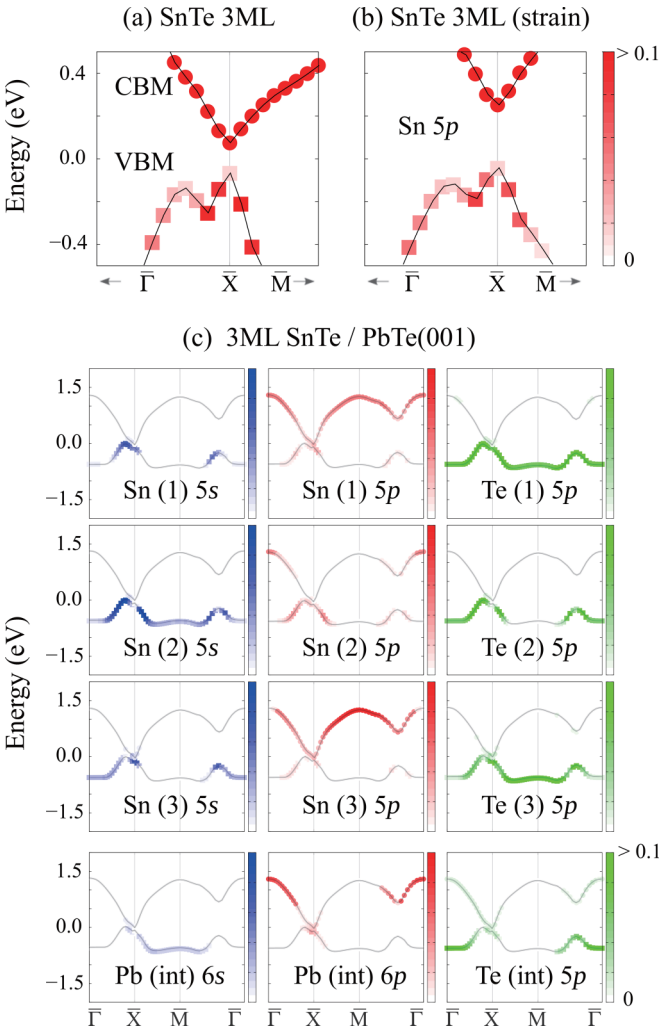

FIG. 8. (Color online) Projected band structure of (a) 3 ML SnTe pristine structure, (b) strained 3 ML SnTe pristine, (c) coherently adsorbed 3 ML SnTe thin film on PbTe(001). The highest occupied state is set to 0 eV. Only CBM and VBM of the crystal orbitals are shown; the contribution weight from each projected orbital to the total wave function is expressed by the color depth of markers. (Squares for VBM; circles for CBM.)

of the nanofilm. However, when the PbTe(001) substrate is considered, with the same magnitude of the expansive strain, SnTe on PbTe(001) shows a more narrow (if not metallic) band gap. While the presence of surfaces in the pristine thin film opened the band gap, the formation of SnTe/PbTe(001) interface resulted in narrower band gap. Therefore, we attribute this to the interface effect as seen from the charge density difference results of SnTe/PbTe(001), where strong charge accumulation in the interface regime is found. From a practical point of view, the Fermi level of this system is predicted to be located near the narrowed band gap. This is consistent with other tight binding model calculation [31]. This special feature suggests that the composite system might be a great candidate for a realization in actual devices.

IV. CONCLUSION

In this work, we considered heteroepitaxy of IV-VI semiconductors with PbTe(001) as a substrate, calculating a number of important mechanical and electronic properties, including the binding energy, formation energy, and work function shifting effects using first-principles DFT. The results demonstrate the close link between the chemical composition, geometric, and electronic structures of the interfaces. We find that the change in work function depends strongly on the cation and the preferred crystal phase of the capping layer. We show that capping layers with Sn cations result in almost monotonic changes in work function with layer thickness, whilst those with Pb cations show a strong oscillatory behavior depending on the number of layers. Additionally, capping layers with the same crystal structure as the substrate result in negative work function changes, whilst those with different preferred crystal phases result in positive shifts in work function for ultrathin film capping layers. We focus on the SnTe/PbTe(001) system and report its unique electronic structure changes at the interface. The results demonstrate how the composition of the capping layer may be tuned in order to achieve different effects in the properties of the substrate, depending on the desired effects and assist with the rational design of such systems for a number of important technological applications, e.g., topological insulator-based devices.

ACKNOWLEDGMENTS

We gratefully acknowledge support by the Global Frontier R&D Program (Grant No. 2013M3A6B1078881) on Center for Global Frontier Hybrid Interface Materials (GFHIM) funded by the Korean Ministry of Science, ICT&Future Planning. This work was also supported by the third Stage of Brain Korea 21 Plus Project Division of Creative Materials. Computational resources have been provided by the Australian National Computational Infrastructure (NCI) and by the KISTI supercomputing center (Grant No. KSC-2013-C3-040). A.W. and K.T.B. acknowledge membership of the UK's HPC Materials Chemistry Consortium, support from the EPSRC Grant, and the Materials Design Network.

[1] H. Zogg, A. Fach, J. John, J. Masek, P. Mueller, C. Paglino, and S. Blunier, Opt. Eng. **34**, 1964 (1995).
[2] F. Wise, Acc. Chem. Res. **33**, 773 (2000).
[3] T. Harman, P. Taylor, D. Spears, and M. Walsh, J. Electron. Mater. **29**, L1 (2000).
[4] G. Springholz, V. Holy, M. Pinczolits, and G. Bauer, Science **282**, 734 (1998).
[5] S. Sawada and K. Nakamura, J. Phys. C **12**, 1183 (1979).
[6] A. A. Lazarides, C. B. Duke, A. Paton, and A. Kahn, Phys. Rev. B **52**, 14895 (1995).
[7] J. Ma, Y. Jia, Y. Song, E. Liang, L. Wu, F. Wang, X. Wang, and X. Hu, Surf. Sci. **551**, 91 (2004).
[8] G. Springholz and K. Wiesauer, Phys. Rev. Lett. **88**, 015507 (2001).

[9] E. Rogacheva, S. Grigorov, O. Nashchekina, T. Tavrina, S. Lyubchenko, A. Sipatov, V. Volobuev, A. Fedorov, and M. Dresselhaus, Thin Solid Films **493**, 41 (2005).
[10] K. Biswas, J. He, Q. Zhang, G. Wang, C. Uher, V. Dravid, and M. Kanatzidis, Nat. Chem. **3**, 160 (2011).
[11] K. Biswas, J. He, I. Blum, C. Wu, T. Hogan, D. Seidman, V. Dravid, and M. Kanatzidis, Nature (London) **489**, 414 (2012).
[12] W. Kohn and L. J. Sham, Phys. Rev. **137**, A1697 (1965).
[13] J. P. Perdew, K. Burke, and M. Ernzerhof, Phys. Rev. Lett. **77**, 3865 (1996).
[14] G. Kresse and J. Furthmüller, Phys. Rev. B **54**, 11169 (1996).
[15] G. Kresse and J. Furthmüller, Comput. Mater. Sci. **6**, 15 (1996).
[16] P. E. Blöchl, Phys. Rev. B **50**, 17953 (1994).
[17] G. Kresse and D. Joubert, Phys. Rev. B **59**, 1758 (1999).
[18] T. Chattopadhyay, J. Pannetier, and H. V. Schnering, J. Phys. Chem. Solids **47**, 879 (1986).
[19] H. Monkhorst and J. Pack, Phys. Rev. B **13**, 5188 (1976).
[20] C. Stampfl and A. Freeman, Appl. Surf. Sci. **258**, 5638 (2012).
[21] R. Wyckoff, Interscience **1**, 85 (1963).
[22] S.-H. Wei and A. Zunger, Phys. Rev. B **55**, 13605 (1997).
[23] A. Walsh and G. W. Watson, J. Phys. Chem. B **109**, 18868 (2005).
[24] N. Dantas, A. Silva, and C. Persson, Opt. Mater. **30**, 1451 (2008).
[25] Y. Zhang, X. Ke, C. Chen, J. Yang, and P. R. C. Kent, Phys. Rev. B **80**, 024304 (2009).
[26] J. M. Skelton, S. C. Parker, A. Togo, I. Tanaka, and A. Walsh, Phys. Rev. B **89**, 205203 (2014).
[27] G. Springholz, M. Pinczolits, V. Holy, S. Zerlauth, I. Vavra, and G. Bauer, Phys. E **9**, 149 (2001).
[28] G. Springholz, V. Holy, P. Mayer, M. Pinczolits, A. Raab, R. T. Lechner, G. Bauer, H. Kang, and L. Salamanca-Riba, Mater. Sci. Eng., B **88**, 143 (2002).
[29] J. He, I. Blum, H. Wang, S. Girard, J. Doak, L. Zhao, J. Zheng, G. Casillas, C. Wolverton, and M. Jose-Yacaman, Nano Lett. **12**, 5979 (2012).
[30] A. Lazarides, C. Duke, A. Paton, and A. Kahn, J. Vac. Sci. Technol. A **13**, 1378 (1995).
[31] J. Liu, T. Hsieh, P. Wei, W. Duan, J. Moodera, and L. Fu, Nat. Mater. **13**, 178 (2014).
[32] C. Li, T. Winzer, A. Walsh, B. Yan, C. Stampfl, and A. Soon, Phys. Rev. B **90**, 075438 (2014).
[33] G. Yang, J. Liu, L. Fu, W. Duan, and C. Liu, Phys. Rev. B **89**, 085312 (2014).
[34] K. T. Butler and A. Walsh, Thin Solid Films **559**, 64 (2014).
[35] L. Fu and C. L. Kane, Phys. Rev. B **76**, 045302 (2007).